

ANOTHER COLLISION FOR THE COMA CLUSTER

A. VIKHLININ, W. FORMAN, AND C. JONES

Harvard-Smithsonian Center for Astrophysics, 60 Garden street, Cambridge, MA 02138, USA.
 e-mail: avikhlinin@cfa.harvard.edu, wforman@cfa.harvard.edu, cjones@cfa.harvard.edu

ABSTRACT

We describe a wavelet transform analysis of the ROSAT PSPC images of the Coma cluster. On small scales, $\leq 1'$, the wavelet analysis shows substructure dominated by two extended sources surrounding the two brightest cluster galaxies NGC 4874 and NGC 4889. On slightly larger scales, $\sim 2'$, the wavelet analysis reveals a filament of X-ray emission originating near the cluster center, curving to the south and east for $\sim 25'$ in the direction of the galaxy NGC 4911, and ending near the galaxy NGC 4921. These results extend earlier ROSAT observations and further indicate the complex nature of the cluster core. We consider two possible explanations for the production of the filamentary feature as arising from interactions of the main cluster with a merging group. The feature could arise from either ram pressure stripped gas or a dark matter perturbation of tidally stripped material.

Subject headings: galaxies: clusters — galaxies: ISM — X-rays: galaxies

1. INTRODUCTION

Clusters of galaxies have relatively long dynamical time-scales, comparable to the age of universe, and hence can provide insights into the conditions and properties of the universe from which these massive systems arose. The study of substructure in clusters has been applied to deriving cosmological parameters (Richstone, Loeb & Turner 1992; Kaufman & White 1993; Lacey & Cole 1993; Mohr et al. 1995). In principle, statistical studies of substructure can provide strong constraints on the density of the Universe, although uncertainties remain including the time-scale for substructure to be erased and the nature of the initial mass fluctuation spectrum (Kaufman & White 1993).

The Coma cluster, as the second X-ray brightest cluster and one of the nearest rich clusters, can provide insights into the reliability of estimates of Ω from substructure studies. Long-considered as the typical dynamically relaxed system, X-ray studies have shown its remarkable complexity (Briel et al. 1992; White, Briel & Henry 1993; Vikhlinin, Forman & Jones 1994). Optical indications of substructure come from the work of Fitchett & Webster (1987) who demonstrated the presence of substructure and Mellier et al. (1988) who were able to derive the mass to light ratios for the core substructures surrounding the two dominant core galaxies. Most recently, Colless and Dunn (1995) used a sample of 552 galaxy redshifts to further clarify the merger history of the Coma cluster. Biviano et al. (1996) combined ROSAT and extensive optical redshift and photometric samples to identify the main body of the cluster and suggested that the main cluster body was undergoing rotation. They also concluded, based on the difference in velocity between the NGC 4889 and NGC 4874 groups and the cluster mean, that these groups only recently arrived within the cluster core.

We have revisited the extensive ROSAT PSPC archival data for the Coma cluster using a new technique, particu-

larly well-suited to detecting small scale structures embedded within larger scale features. This technique, “wavelet transform decomposition”, allows simultaneous study of the image at all spatial (angular) scales and allows identification of the scale appropriate to the detected features. In this *Letter*, we study the small scale structure of the Coma image with this new wavelet transform technique. We detect a long, narrow X-ray feature and discuss possible explanations as either gas which was ram pressure stripped from a small galaxy group during a recent merger/collision with the cluster or a dark matter perturbation produced by tidally stripped material during a group merger.

2. OBSERVATIONS AND ANALYSIS

We analyzed two ROSAT PSPC pointings of the Coma cluster core (the overall X-ray morphology of the Coma cluster seen from pointed ROSAT observations is discussed in White et al. 1993). Images were reduced using the prescriptions and code of Snowden et al. (1994). This includes the elimination of high background intervals, which are primarily due to intense scattered solar X-rays, subtraction of the particle and other non-cosmic background components¹, and creation of the exposure maps appropriate for the given energy band which are used for flat-fielding and merging the images obtained from different pointings. The cleaning resulted in 18 and 13 ksec exposures in individual pointings. The merged PSPC image (top-left panel in Fig 1) shows an azimuthally asymmetric cluster (Briel et al. 1992, White et al. 1993) whose core structure we investigate in detail in this *Letter*.

2.1. Wavelet Decomposition

The technique we applied to the ROSAT PSPC “cleaned” images employs a set of *à trous* wavelet transforms, closely following the approach of Starck et al. (1995 and references therein) with some important changes

¹The so-called “long term enhancement” (see explanations in Snowden et al.) and the residual solar scattered X-rays

in the iteration scheme. An application of the multi-resolution wavelet-based image filtering for the X-ray images also can be found in Slezak et al. (1994).

The *à trous* wavelet transform of scale a can be (very roughly) characterized as the convolution of an image with the function equal to the difference between two Gaussians, the first positive one with $\sigma = a$, and the second negative one with $\sigma = 2a$. The basic idea of the wavelet-based image filtering is to perform the set of wavelet transforms with scales $a, 2a, 4a, \dots$, retain only significant wavelet coefficients at each scale (thus filtering out the noise), and perform the image reconstruction from the wavelet planes. For the *à trous* wavelet transform, the reconstruction is performed by simple summation of all wavelet planes. At each scale we retain the wavelet coefficients which exceed some critical amplitude which corresponds to the given number of standard deviations (3σ in our application). Since the wavelet transform is linear, the noise level in each wavelet plane is proportional to the noise level in the original image. Therefore, we can derive the critical amplitudes for each scale using the following approach. We first apply the wavelet transform to a simulated image containing Gaussian noise with dispersion 1 and determine the *rms* variations in the wavelet-convolved images. We then multiply these values by the local noise in the actual image, which is estimated using the local background and exposure. Thus, the faintest detectable structures have uniform amplitude in terms of significance, as a function of both position and scale.

To assure the most complete separation of image features in terms of their scale, we apply the following iterative procedure. We start from the smallest scale, $a = 30''$, which roughly corresponds to the FWHM of the ROSAT PSPC PSF. We calculate the wavelet transform on this first scale only, find significant features, and subtract them from the original image (recall that the back-transformation for the *à trous* wavelet transform is simply the summation of the wavelet planes). The next iteration is applied to the residual and this process is repeated until no new significant features are found at this scale. We then start the process with the scale $2a$ and so on. The subtraction of the features detected at smaller scales before applying the wavelet transform at larger scales results in a sufficient enhancement of the basic property of the wavelet transform analysis — its ability to separate image features in terms of their characteristic scale. In particular, we are able to isolate even extremely bright point sources primarily at the two smaller scales (i.e. $\leq 60''$), whereas without subtraction, they appear at all scales and often saturate nearby and relatively faint extended structures.

The process described above provides a separation of the original image into a set of images containing only features of scale $a, 2a, \dots$ significant at least at the 3σ level, which can be either summed together to produce an adaptively smoothed image or viewed individually (or in any desired combination) to examine the significant structures at desired scales.

2.2. Small Scale Structure of the Coma Cluster

Contour maps of the images generated for small scales are shown in the bottom panels of Fig 1 superposed on an optical image. On the smallest scales, $60''$ (*bottom-left*), the contours show the extended sources surrounding the two brightest cluster galaxies NGC 4874 and NGC 4889 first detected in X-rays by White et al. (1993; see also Vikhlinin et al. 1994). On larger scales, $120''$ (*bottom-right*), the wavelet analysis reveals a filamentary X-ray emission feature originating near the cluster center, curving to the south and east for $\sim 25'$ towards the galaxy NGC 4911, and ending near the galaxy NGC 4921. The surface brightness enhancement near NGC 4911 was first noted by White et al. (1993).

Within the outer contour of the filament, the surface brightness ranges from 5–10% of the underlying diffuse emission from Coma itself. The formal significance along the axis of the filament varies from 4.5σ to 6σ . Features with this significance never appear in simulated Coma cluster images. The counts associated with the emission filament (within the outer contour shown in bottom-right panel of Fig 1) correspond to a count rate of 0.12 cts s^{-1} in the energy band 0.5–2 keV. The corresponding luminosity, for $H_0 = 50 \text{ km sec}^{-1} \text{ Mpc}^{-1}$ and a sufficiently hard spectrum (see below) is $3 \times 10^{42} \text{ ergs sec}^{-1}$. At the Coma distance ($z = 0.0235$), the tail is approximately 1 Mpc ($25'$) in length with a diameter of 160 kpc ($4'$).

It is interesting to constrain the spectral properties of the filamentary structure. It is faint compared to the underlying cluster emission, which therefore cannot be neglected and must be carefully subtracted. We use the following technique for the extraction of the filament's spectrum. We perform the wavelet decomposition of the broad band image as described above and record all the transformations which have been applied. The identical transformations are performed to the images in individual energy bands defined by the energies 0.2–0.4–0.5–0.7–0.9–1.3–2 keV. Since the wavelet transform is linear, the relative fluxes in different energy bands are conserved and can be used to fit the spectrum. Unfortunately, there is a serious problem with the PSPC spectral calibration for these particular observations, which results in anomalously low temperatures for the total cluster emission.² We therefore use the ratio of the filament brightness to the underlying cluster brightness as a function of energy to constrain the filament spectrum. This ratio is constant within the errors, which suggests that the filament has the same spectrum as the Coma cluster. Quantitatively, a 95% lower limit to the temperature in the filament is 4 keV, assuming a cluster core temperature of 8 keV (Hughes, Gorenstein & Fabricant 1988).

3. DISCUSSION

The wavelet analysis of the ROSAT PSPC X-ray images of the Coma cluster demonstrates the existence of a new feature possibly associated with dynamical activity in the cluster core. We can estimate the physical parameters associated with this filament of emission assuming it arises from hot gas. Let us assume that we are viewing the filament in the plane of the sky and it is a uniform cylin-

²To our knowledge, a similar effect is found for other clusters observed around July 1991: A3558 (Markevitch & Vikhlinin 1997) and A1795 (L. David, private communication), have anomalously low best fit temperatures. This suggests that a likely explanation is a detector gain variation around July 1991, which is not accounted for by the present versions of the PSPC calibration.

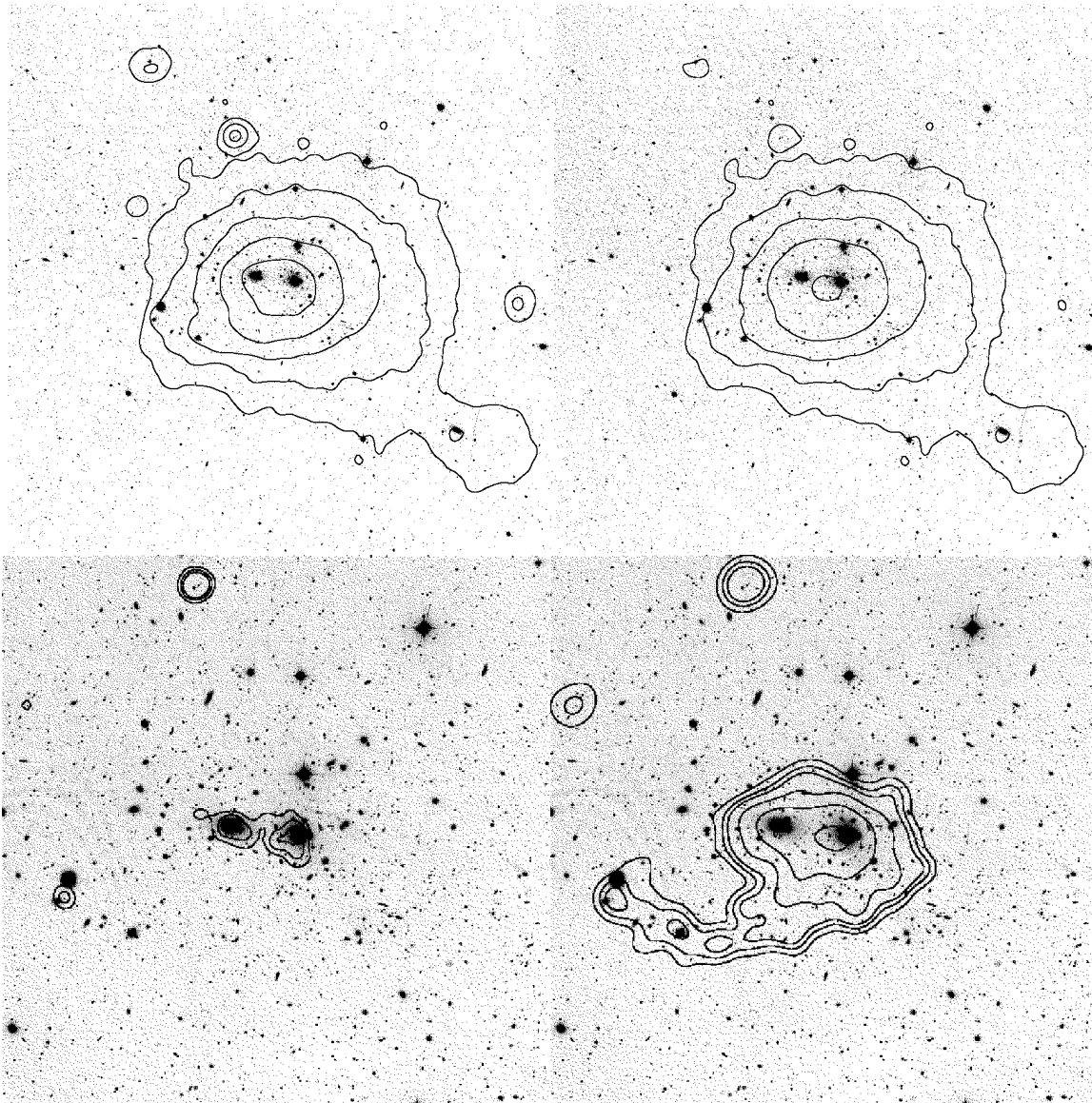


FIG. 1.—(top-left) The X-ray image of the Coma cluster in the energy band 0.5–2 keV, smoothed with the Gaussian $\sigma = 1'$, overlaid on the optical image. (bottom-left) Structure detected in the Coma cluster core on the wavelet scale $60''$. The most prominent features are extended sources around NGC 4889 and NGC 4874, as well as a few point sources. (bottom-right) Structure detected on the $120''$ scale. The tail of enhanced emission originates near NGC 4874, goes to the South and East towards NGC 4911 and ends near NGC 4921. The formal statistical significance along the axis of the tail varies from 4.5σ to 6σ , and the surface brightness is $\sim 10\%$ of the underlying cluster emission. (top-right) Small scale structures shown in bottom panels were subtracted from the Coma cluster image, and the result was smoothed with the Gaussian $\sigma = 1'$. After the subtraction of the small-scale structure the cluster core appears much more regular. The complex morphology (elongation, and the rotation of the elongation axis) therefore reflects the “hidden” small-scale structure, not the state of the main cluster body.

der of radius 100 kpc and length 1 Mpc. The observed 10% surface brightness enhancement implies that the density of the filament must exceed the cluster gas density at least by about 5%, if the gas is not particularly cool ($T >$ a few keV). The relative brightness of the filament does not change much along its axis, therefore the gas density enhancement in the filament is an almost constant small perturbation and one can use the main cluster density profile (Briel et al. 1992) to estimate the filament’s gas mass. We derive a total average gas density in the volume defined by the filament of approximately 10^{-3} cm^{-3} with a range (along the filament’s axis) from about 2.5×10^{-4} to $2.5 \times 10^{-3} \text{ cm}^{-3}$. This density translates into a gas mass

of $5 \times 10^{11} M_{\odot}$. We consider two possible scenarios for the origin of this filamentary feature.

First, let us suppose that this feature arises from gas that has been ram pressure stripped from a merging group. The observed gas mass is well within the reasonable range for the gas mass in the core of a group (see for example, Fig 4 of David et al. 1995). More importantly, however, we must consider whether such a thin structure could survive in the cluster environment. Following Cowie & McKee (1977), we have computed the evaporation rate for a spherical cloud embedded in the hot ICM of the Coma cluster. In the Coma cluster core, the classical thermal conduction should provide a reasonable estimate for the

evaporation time, which is given as

$$t_{\text{evap}} = 3.3 \times 10^{20} n_c R_{\text{pc}}^2 T_f^{-5/2} (\ln \Lambda / 30) \text{ yr}, \quad (1)$$

where n_c is the embedded cloud density, R_{pc} is its radius in pc, T_f is the temperature of the surrounding, hot medium, and Λ is the Coulomb logarithm. For a cloud of radius 10^2 kpc, density $2.5 \times 10^{-3} \text{ cm}^{-3}$, embedded in a hot medium of temperature 8 keV, the evaporation time is $t_{\text{evap}} \sim 0.1$ Gyr. In 0.1 Gyr, a galaxy or group traveling at the cluster velocity dispersion could traverse 0.2 Mpc. The evaporation time at the end of the filament away from the cluster center where its density is lower is significantly shorter. In principle, cylindrical geometry makes the evaporation time longer by a factor of a few. Also, any chaotic magnetic field could significantly reduce the thermal conduction efficiency and increase the evaporation time-scale. Finally, we do not necessarily need the evaporation time-scale to be smaller or comparable to the traverse time: if the amount of gas deposited into the tail significantly exceeded $5 \times 10^{11} M_{\odot}$, it may be mostly evaporated at present, with only the remnants of the group gas providing the observed surface brightness enhancement.

An alternative is that the observed filamentary feature arises from cluster gas compressed in the potential well of the dark matter perturbation formed by a tidally disrupted infalling galaxy group. Merritt (1984) has shown that galaxy halos are tidally disrupted by the cluster gravitational field. Specifically, a gravitationally bound system entering a cluster is tidally limited at a radius r_t given by:

$$r_t / R_c = F(r / R_c) \sigma_g / \sigma_c \quad (2)$$

where R_c is the cluster core radius, σ_g is the group velocity dispersion, σ_c is the cluster velocity dispersion, r is the distance from the cluster center, and $F(r / R_c)$ is a function which has a minimum value of $1/2$ at $r = R_c$ (see Fig 1 in Merritt 1984). The function $F(r / R_c)$ decreases nearly linearly with decreasing radius and hence an infalling group will be tidally disrupted as it approaches $r = R_c$. The minimum size depends in detail on the parameters of the group and cluster, but for a typical group with $\sigma_g = 300 \text{ km sec}^{-1}$ in the Coma cluster with $\sigma_c = 1142 \text{ km sec}^{-1}$ (Biviano et al. 1996) and $R_c = 420 \text{ kpc}$ (Briel et al. 1992), the maximum tidal radius for an infalling group is $r_t \sim 50 \text{ kpc}$. Thus, the group will be progressively disrupted as it approaches the core. A trail of tidally stripped debris behind the group provides the gravitational potential perturbation which enhances the surface brightness. For isothermal gas in hydrostatic equilibrium, the gas density perturbation is:

$$(\rho_0 + \delta\rho) / \rho_0 = \exp(-\mu m_p \Delta\varphi / kT). \quad (3)$$

where ρ_0 is the initial gas density, and kT is the gas temperature. The observed surface brightness enhancement corresponds to a gas density enhancement of about 5%, hence the change in the gravitational potential, $\Delta\varphi$, can be written as $1.05 = \exp(-\mu m_p \Delta\varphi / kT)$ or $\Delta\varphi = 0.05 kT / \mu m_p$.

The gravitational potential on, and near, the surface of a long cylinder is:

$$\psi = -G\rho_l \ln(L/R) \quad (4)$$

where ρ_l is the linear mass density, L is the length of the cylinder, and R is its radius. If we equate the potential

on the surface of the cylinder to the change in the gravitational potential required to produce the observed surface brightness enhancement, then we can solve for the linear mass density in the cylinder. This provides an expression for the added mass in the cylinder:

$$\rho_l L = \frac{\Delta\varphi L}{G \ln(L/R)} = \frac{0.05 k T L}{\mu m_p G \ln(L/R)} \quad (5)$$

For the observed properties of the filament, and assuming the gas temperature is that of the cluster, we find a mass of $M = 6 \times 10^{12} M_{\odot}$. At most, the mass could be 50% smaller if the temperature of the gas in the filament is at its measured lower limit. The surface brightness enhancement also may be underestimated by a factor of a few, since the filament may not be located in the densest part of the projected gas distribution in which case the required density contrast is larger. Also, the 10% enhancement in the surface brightness corresponds to more than 10% enhancement in the volume emissivity, because the filament is narrow and projected onto the main cluster emission. Thus, the measured mass in the perturbation is approximately $6 \times 10^{12} M_{\odot}$ and is uncertain by a factor of about 2. This mass is well within the range of that in the central region of a group (e.g. David et al. 1995).

We have discussed the filament in some detail, but the remaining emission is also of interest. The top-right panel in Fig 1 compares the “raw” smoothed image of Coma (*top-left*) with the smoothed image after subtraction of the detected small scale structure (*bottom panels*). The removal of the two central X-ray peaks around the galaxies NGC 4889 and NGC 4874, as well as the filament, leaves a smooth and regular-looking X-ray surface brightness distribution. A relatively small surface brightness perturbation can produce marked irregularity in the surface brightness distribution. Therefore, the small scale structure can significantly influence the overall appearance of the surface brightness distribution of the cluster. Numerical simulations must retain sufficient resolution, if they are to fully model shapes of the X-ray cluster images.

4. CONCLUSIONS

We report the detection of a long, linear filamentary feature extending over approximately 1 Mpc from the Coma cluster center toward NGC 4911. We explore two possibilities for the origin of this filament. First, we show that the filament could arise from ram pressure stripped gas from a group passing through Coma, especially if magnetic fields significantly reduce the conduction efficiency and lengthen the evaporation time. Second, we note that tidally stripped dark matter from a merging group could produce a perturbation that would give rise to the observed structure.

Increases in sensitivity and new analysis techniques have continued to demonstrate the complexity of the cluster environment. The Coma cluster, long thought to be the prototype for a relaxed cluster, is in fact a remarkably complex system with structure on many different scales seen both optically and in X-rays.

We thank L. David for helpful discussions and acknowledge support from NAS8-39073.

REFERENCES

- Biviano, A., Durret, F., Gerbal, D., Le Fèvre, O., Lobo, C., Mazure, A., & Slezak, E. 1996, *A&A*, 311, 95.
- Briel, U., Henry, J.P. & Böhringer, H. 1992, *A&A*, 259, L31
- Colless, M. & Dunn, A. 1995, preprint (astro-ph/9508070)
- Cowie, L. & McKee, C. 1977, *ApJ*, 211, 135
- David, L., Jones, C., and Forman, W. 1995, *ApJ*, 445, 578.
- Fitchett, M.J & Webster, R. 1987, *ApJ*, 317, 653
- Hughes, J.P., Gorenstein, P., and Fabricant, D. 1988, *ApJ*, 329, 82
- Kaufman, G. & White, S. 1993, *MNRAS*, 261, 921
- Lacey, C. & Cole, S. 1993, *MNRAS*, 262, 627
- Markevitch, M. & Vikhlinin, A. 1997, *ApJ*, in press astro-ph/9605026
- Merritt, D. 1984, *ApJ*, 276, 26
- Mellier, Y., Mathez, G., Mazure, A., Chauvineau, B. & Proust, D. 1988, *A&A*, 199, 67
- Mohr, J., Fabricant, D. & Geller, M. 1993, *ApJ*, 413, 492
- Richstone, D., Loeb, A. & Turner, E. 1992, *ApJ*, 393, 477
- Slezak, E., Durret, F., & Gerbal, D. 1994, *Ap. J.*, 108, 1996.
- Snowden, S.L., McCammon, D.; Burrows, D.N. & Mendenhall, J.A. 1994, *ApJ*, 424, 714.
- Starck, J.-L., Murtagh, F. & Bijaoui, A., 1995, *ADASS Conf. Proc.*, ASP Conf. Series, 77, 279.
- Vikhlinin, A., Forman, W. & Jones, C. 1995, *ApJ*, 435, 162
- White, S., Briel, U. & Henry, J.P., 1993, *MNRAS*, 261, 8